Electronic Supplementary Material (ESI) for Inorganic Chemistry Frontiers.

ESI

Single-molecule magnetism in $\{Co^{III}_2Dy^{III}_2\}$-amine-polyalcohol-acetylacetonate complexes: Effects of ligand replacement at Dy^{III} on the dynamics of relaxation

Stuart K. Langley,[a] Nicholas F. Chilton,[b] Boujemaa Moubaraki[a] and Keith S. Murray[a*]

[a] ***School of Chemistry, Monash University, Clayton, Victoria 3800, Australia***

[b] ***School of Chemistry, University of Manchester, Manchester M13 9PL, U.K.***

email: keith.murray@monash.edu

Computational details

All CASSCF/RASSI calculations were performed with MOLCAS 7.8. The active space for all complexes consisted of nine electrons the seven 4f orbitals of Dy(III), where the non-active Dy(III) ion was computationally substituted for the diamagnetic Lu(III). For all cases except **3**, the ANO-RCC-VTZP basis set was employed for the Dy(III) ion, while the VDZP basis was used for the first coordination sphere atoms, VDZ for all other non-hydrogen atoms and the MB basis for hydrogen atoms. For **3**, the ANO-RCC-VTZP basis set was used for Dy, the VDZP basis was used for the first coordination sphere atoms, VDZ for all other O, Co and Lu atoms, and the MB basis for C, H and N. 21 sextet states, 224 quartets and 158 doublets were included in the state averaged CASSCF procedure. 21 sextets, 128 quartets and 130 doublets were mixed by spin-orbit coupling in the RASSI procedure.

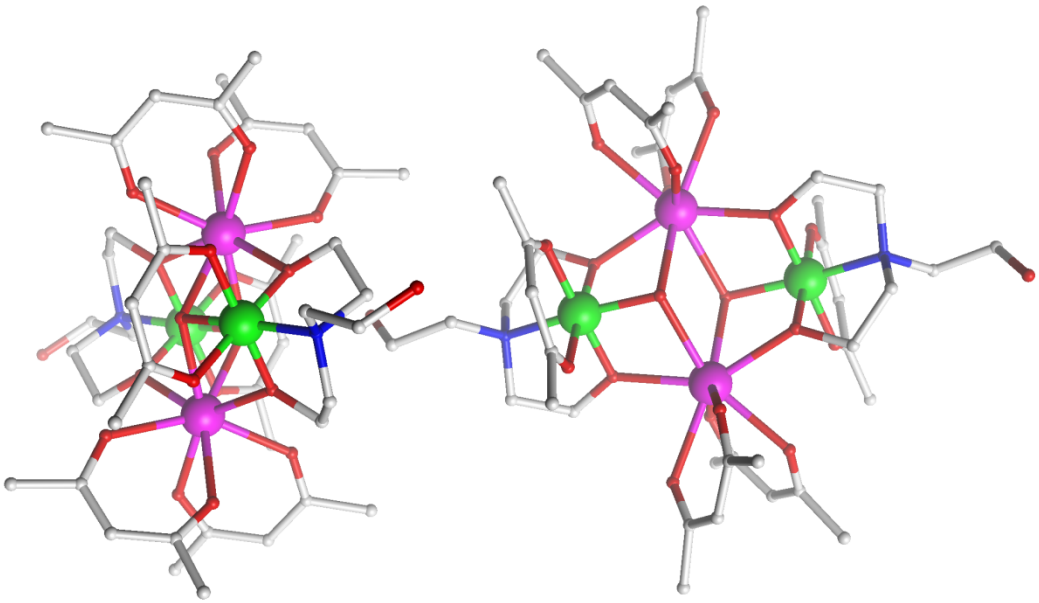

Figure S1. Molecular structure of compound **3**, with two crystallographic unique molecules found in the asymmetric unit. The H-atoms are omitted for clarity. Colour scheme; Co^{III}, Green; Dy^{III}, purple; O, red; N, blue; C, light grey.

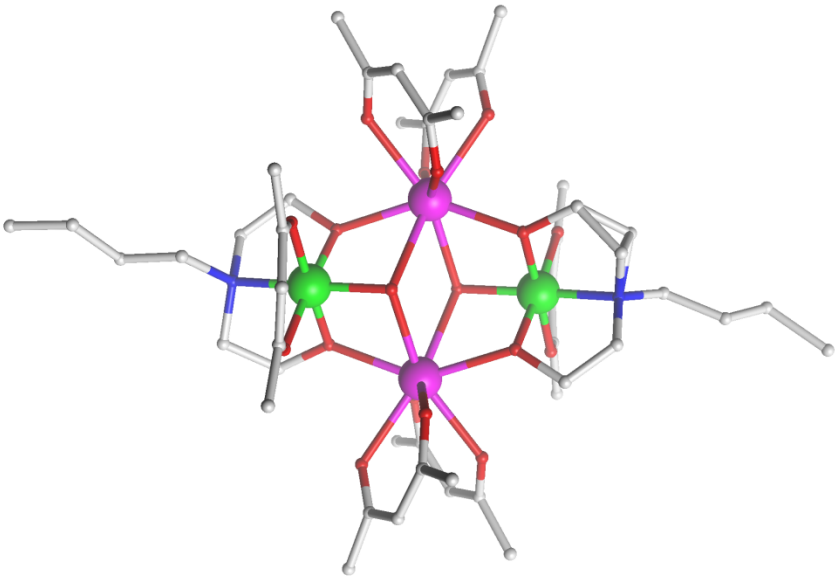

Figure S2. Molecular structure of compound **4**. The H-atoms and the disordered carbon atoms are omitted for clarity. Colour scheme; Co^{III}, Green; Dy^{III}, purple; O, red; N, blue; C, light grey.

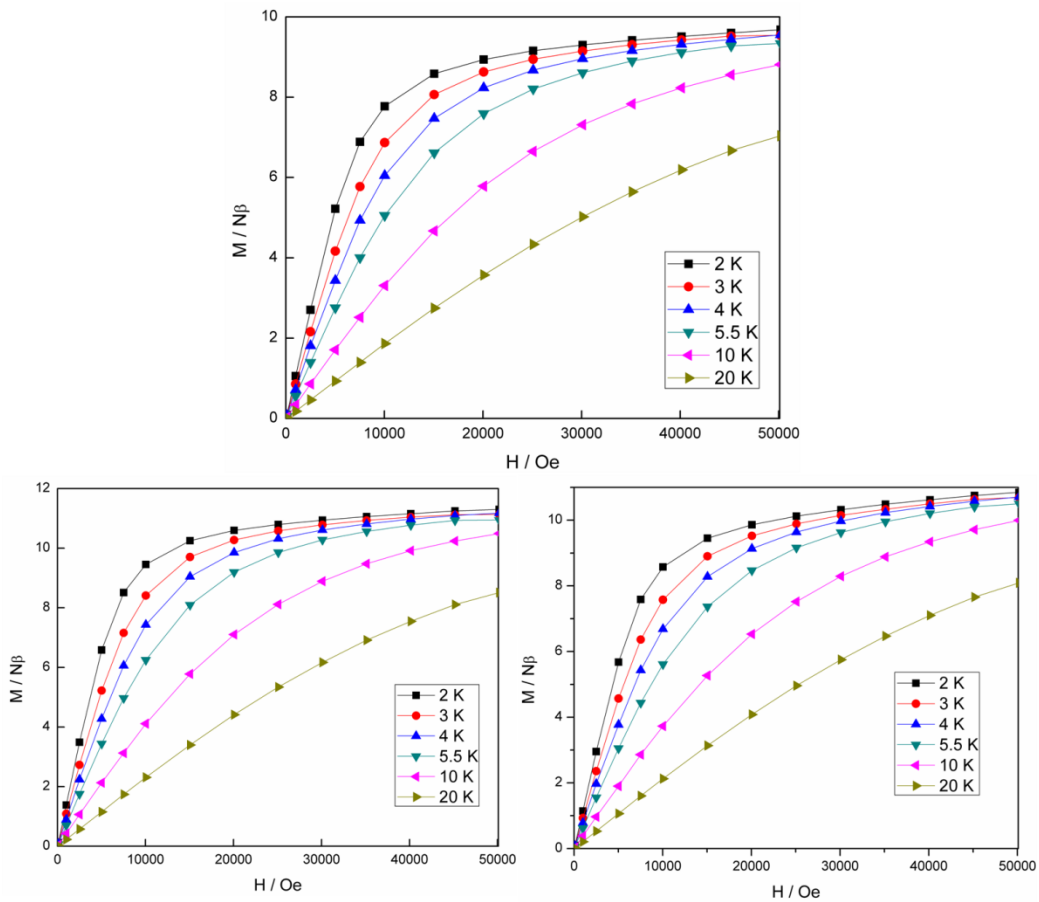

Figure S3. Isothermal *M versus H* plots for **3** (top), **4** (bottom left) and **5** (bottom right).

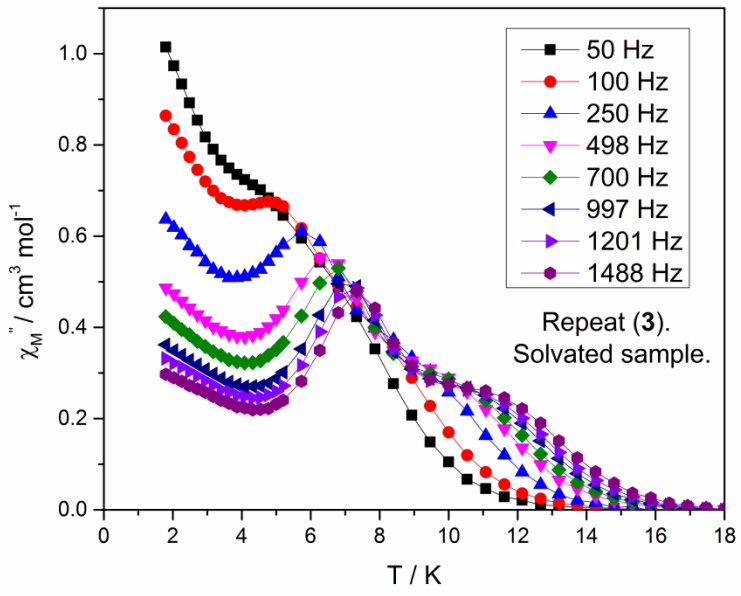

Figure S4. Plot of χ_M'' *versus T* for freshly prepared repeat batch of **3** at H_{dc} = 0 Oe.

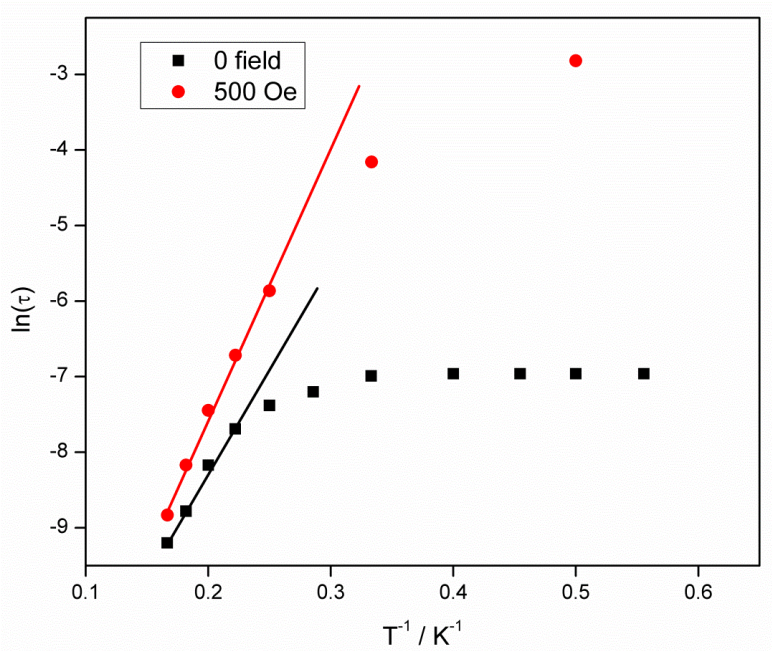

Figure S5. Magnetization relaxation time (τ) plotted as ln(τ) vs T^{-1} for compound **4** at 0 field and 500 Oe. The solid black and red lines represent a fit to the Arrhenius law in the thermally activated regime.

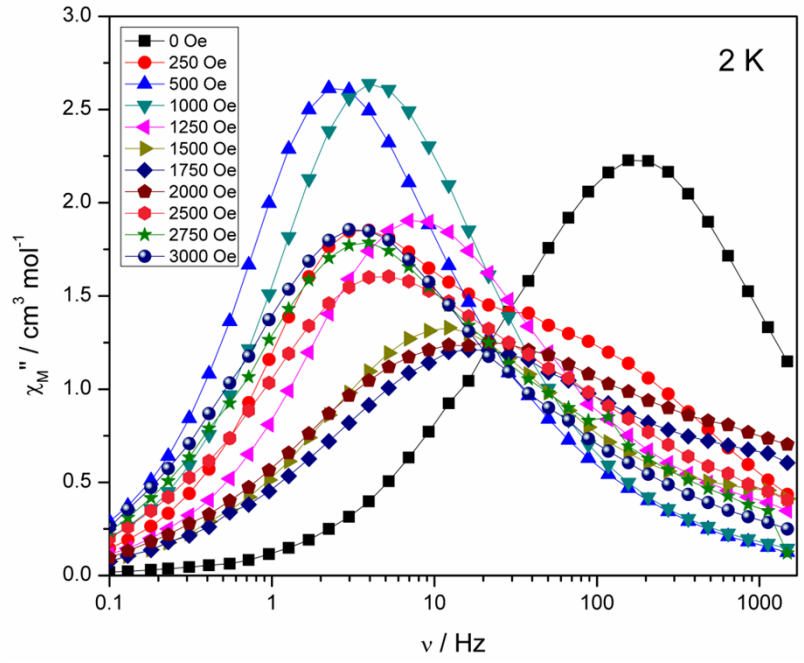

Figure S6. Plot of χ_M'' *versus* frequency at 2 K for **4** under the application of variable dc fields, ranging from 0 to 3000 Oe.

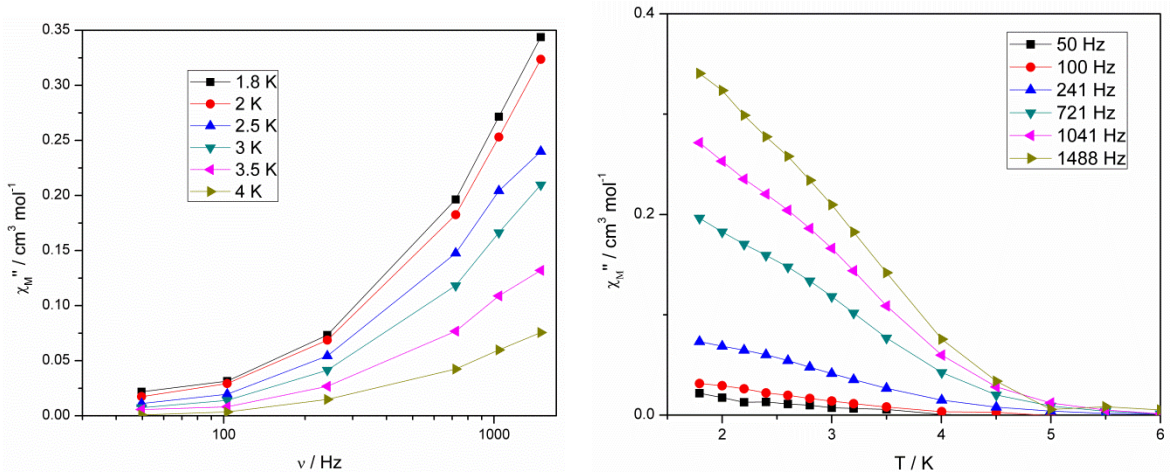

Figure S7. Frequency (left) and temperature (right) dependence of the out-of-phase ac susceptibility, χ_M'', of **5** in zero applied dc magnetic field. The solid lines just join the points.

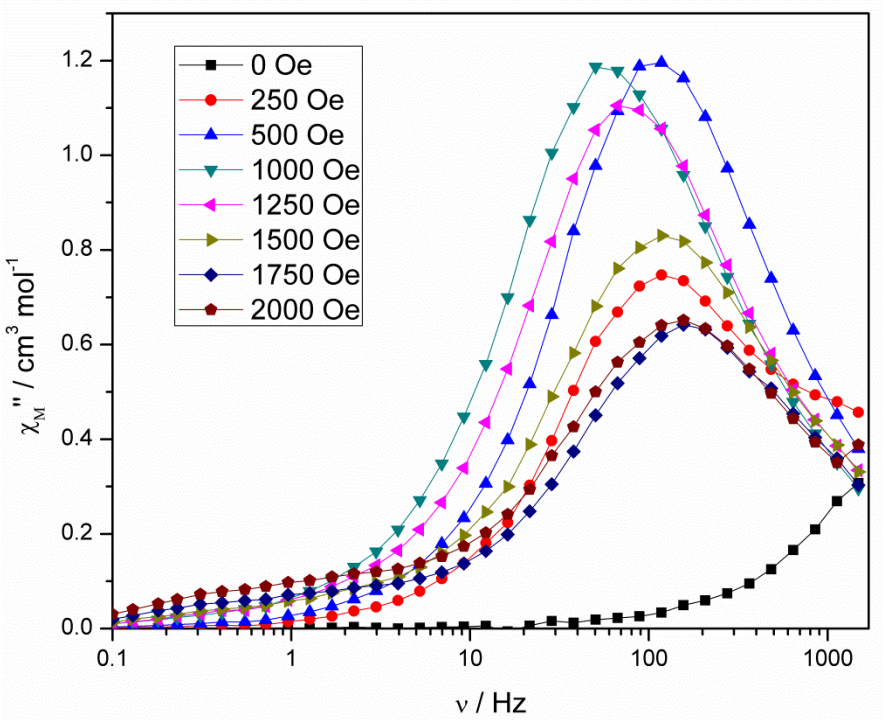

Figure S8. Plot of χ_M'' *versus* frequency at 2 K for **5** under the application of variable dc fields, ranging from 0 to 2000 Oe.

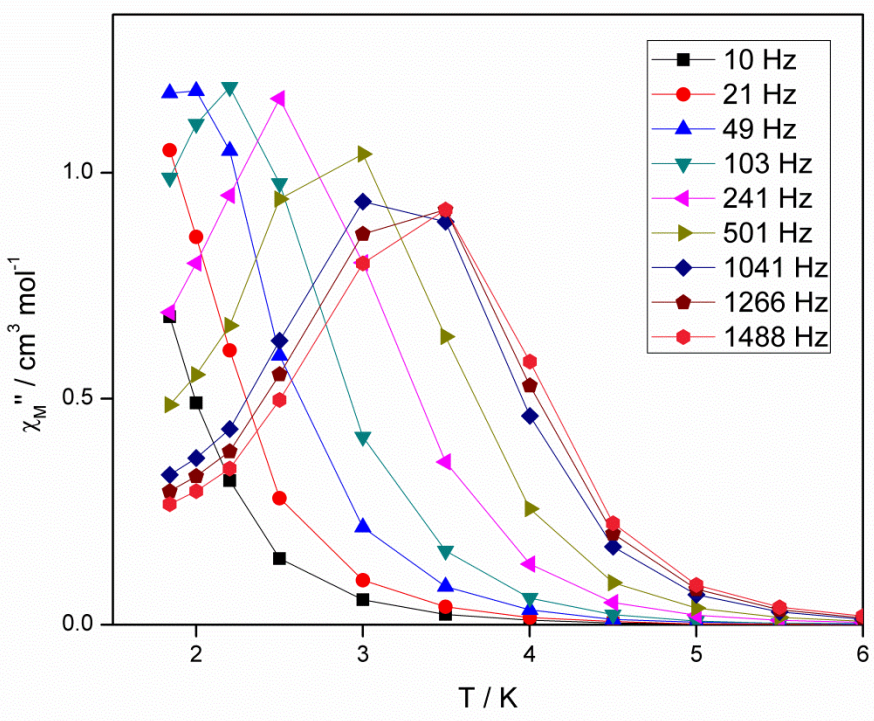

Figure S9. Plot of χ_M'' *versus* T for **5** at H_{dc} = 1000 Oe.

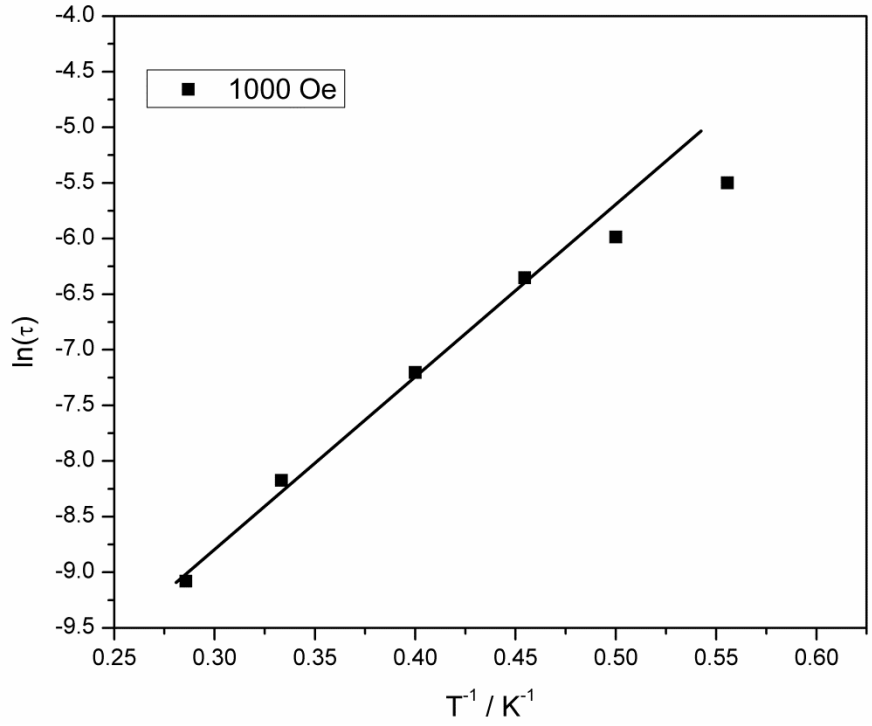

Figure S10. Magnetization relaxation time (τ) plotted as ln(τ) vs T^{-1} for compound **5** at 1000 Oe. The solid black line represents a fit to the Arrhenius law in the thermally activated regime.

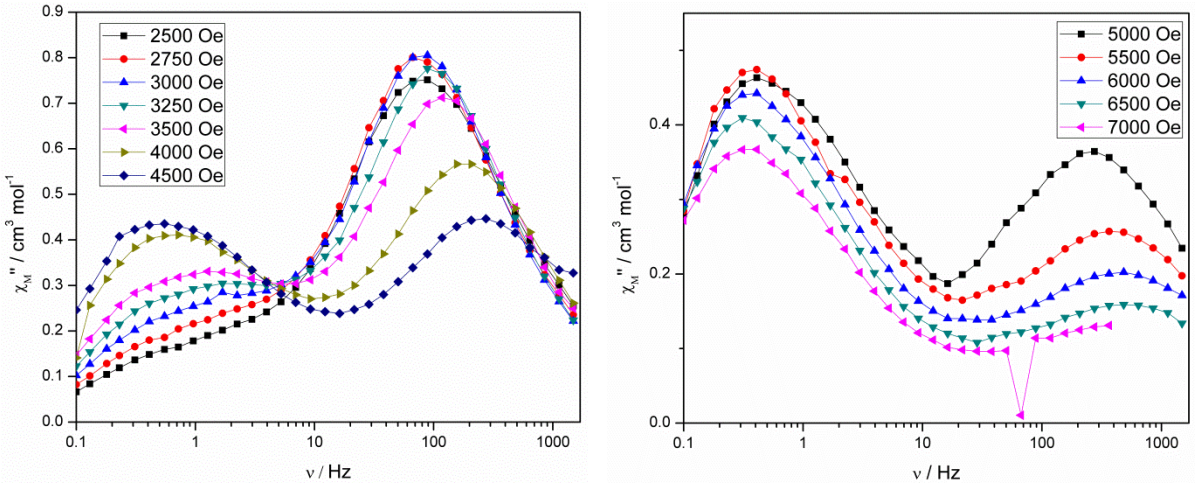

Figure S11. Plot of χ_M'' *versus* frequency at 2 K for **5** under the application of variable dc fields, ranging from 2500 to 4500 Oe (left) and 5000 to 7000 Oe (right).

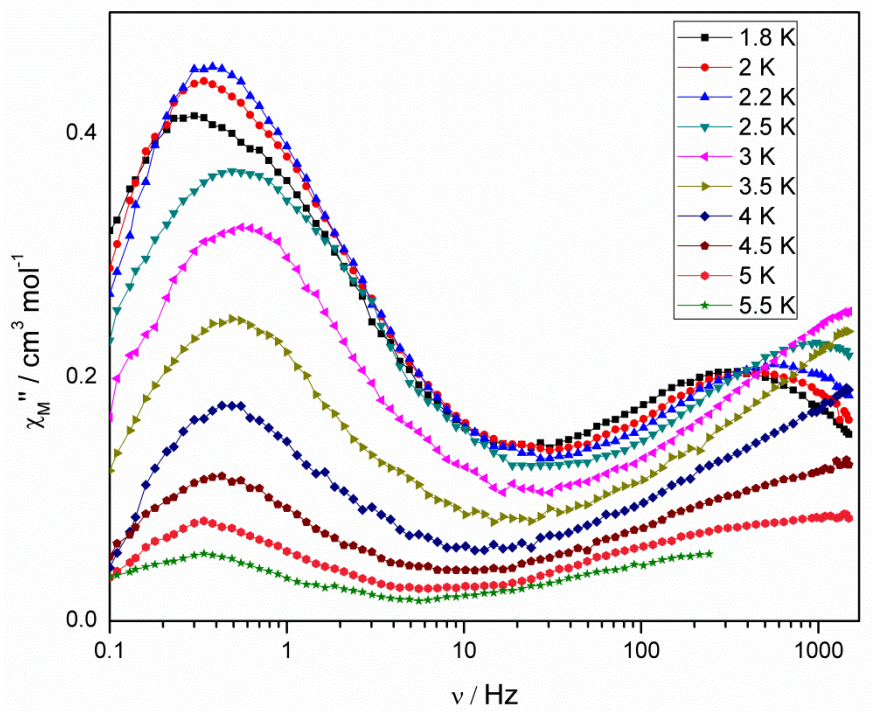

Figure S12. Plot of χ_M'' *versus* frequency for **5** with H_{dc} = 6000 Oe.

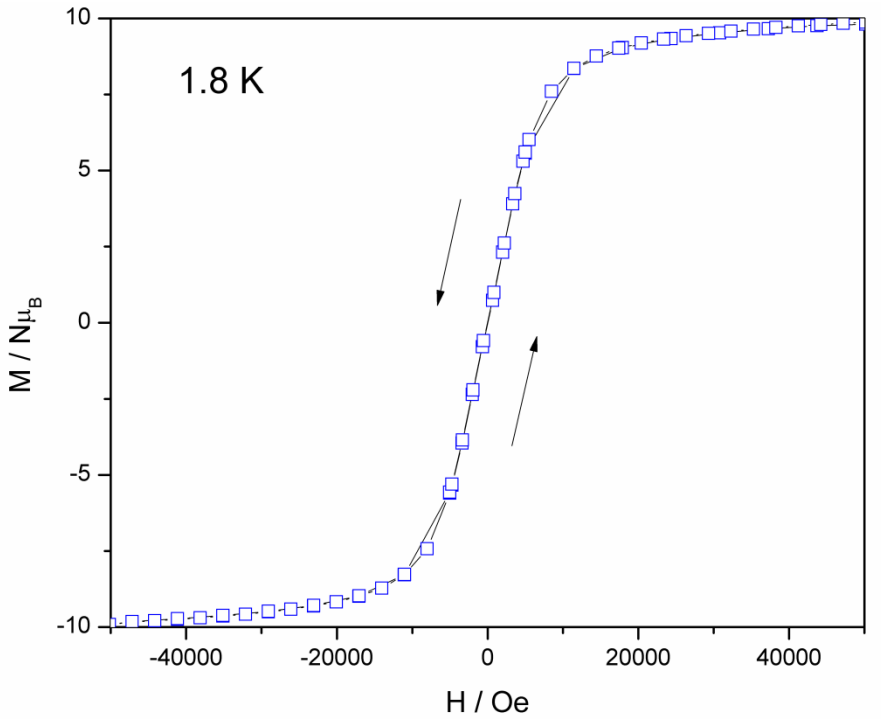

Figure S13. Plot of magnetization (*M*) *versus* field (*H*) for **3**, sweeping the field with an average sweep rate of 0.003 T/s, at 1.8 K.

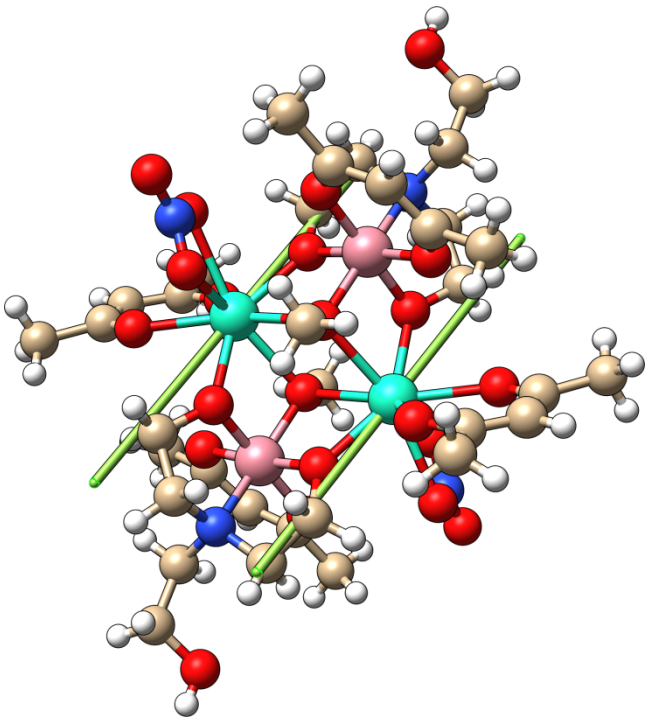

Figure S14. Ground state magnetic anisotropy axes for Dy^{III} sites of **1a** (green rods). Teal = Dy, pink = Co, red = O, blue = N, tan = C, white = H.

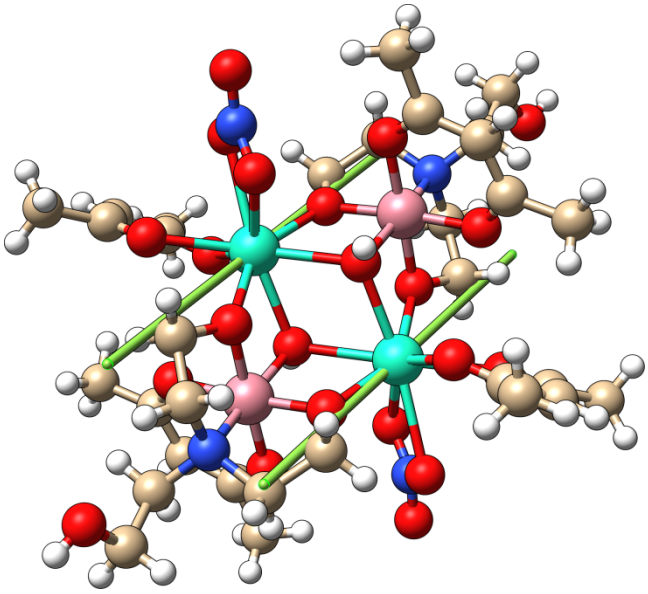

Figure S15. Ground state magnetic anisotropy axes for Dy^{III} sites of **1b** (green rods). Teal = Dy, pink = Co, red = O, blue = N, tan = C, white = H.

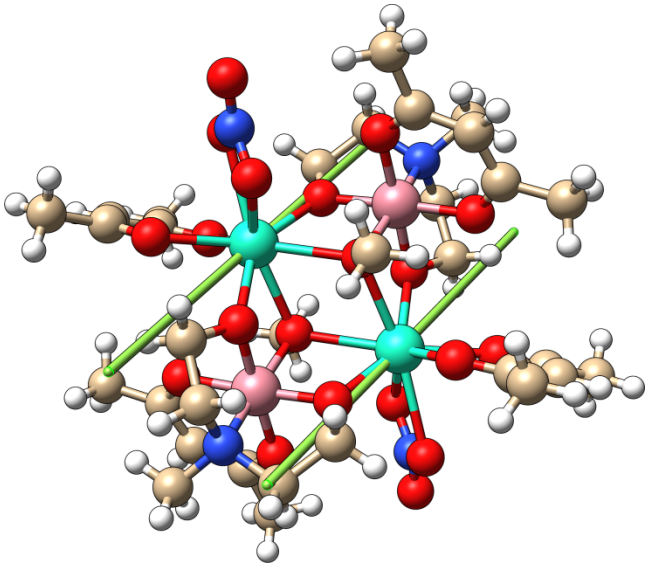

Figure S16. Ground state magnetic anisotropy axes for Dy^{III} sites of **1c** (green rods). Teal = Dy, pink = Co, red = O, blue = N, tan = C, white = H.

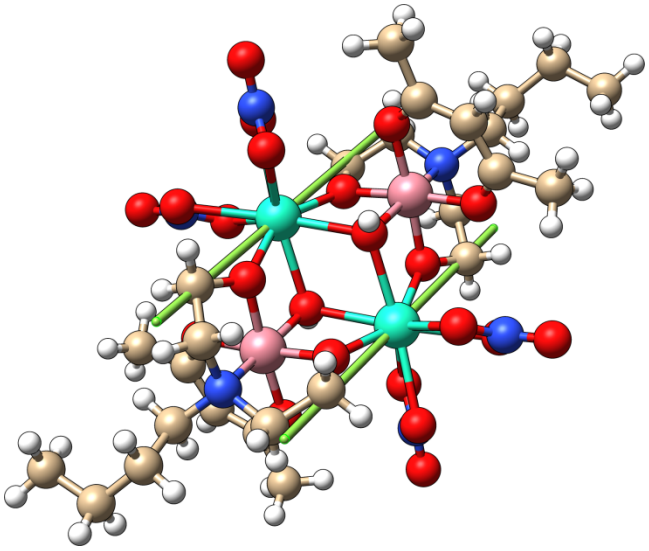

Figure S17. Ground state magnetic anisotropy axes for Dy^{III} sites of **2** (green rods). Teal = Dy, pink = Co, red = O, blue = N, tan = C, white = H.

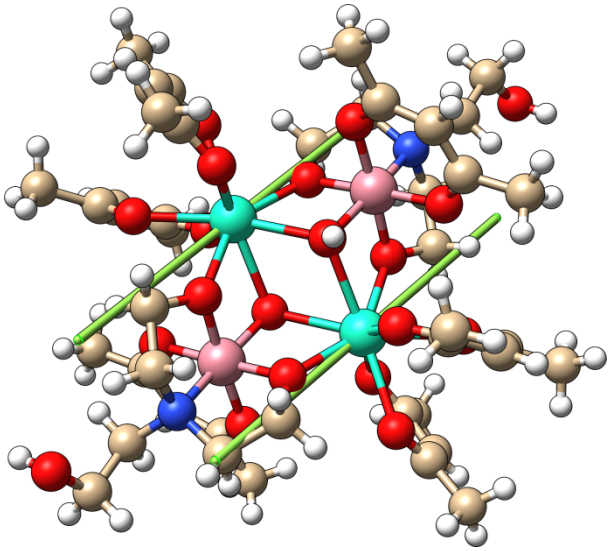

Figure S18. Ground state magnetic anisotropy axes for Dy^{III} sites of **3(Dy1)** (green rods). Teal = Dy, pink = Co, red = O, blue = N, tan = C, white = H.

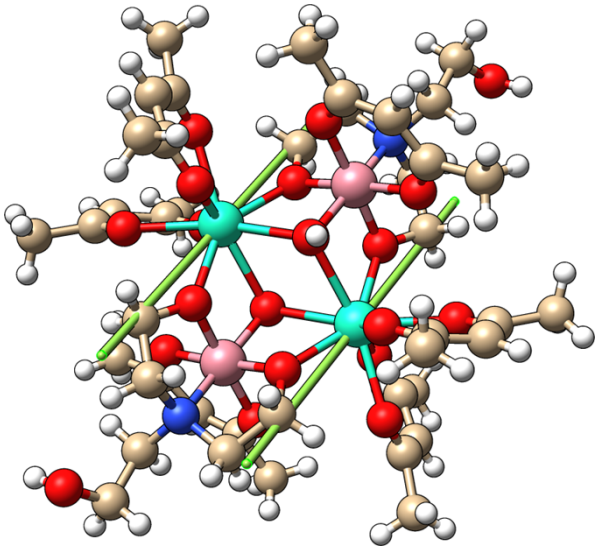

Figure S19. Ground state magnetic anisotropy axes for Dy^{III} sites of **3(Dy2)** (green rods). Teal = Dy, pink = Co, red = O, blue = N, tan = C, white = H.

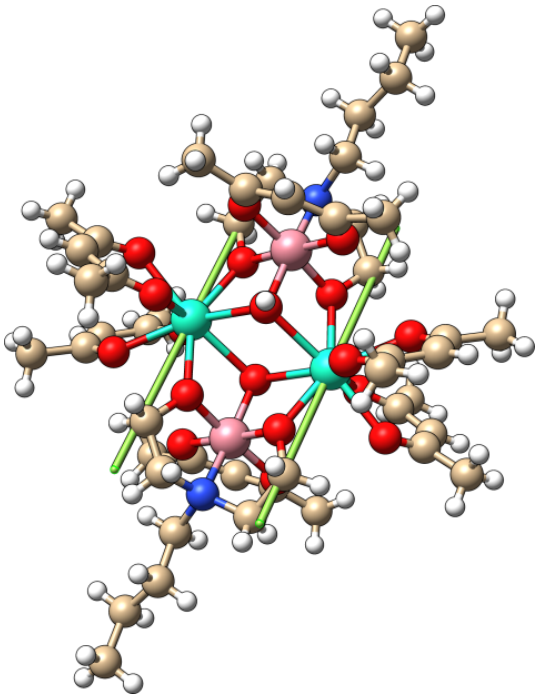

Figure S20. Ground state magnetic anisotropy axes for Dy^{III} sites of **4** (green rods). Teal = Dy, pink = Co, red = O, blue = N, tan = C, white = H.

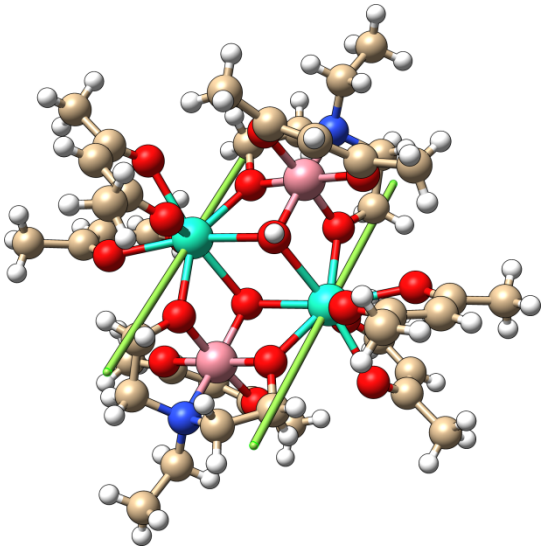

Figure S21. Ground state magnetic anisotropy axes for Dy^{III} sites of **5** (green rods). Teal = Dy, pink = Co, red = O, blue = N, tan = C, white = H.

Table S1. Energy spectrum of $^6H_{15/2}$ multiplet for **1a**.

Energy (cm^{-1})	g_x	g_y	g_z	Angle (°)
0	0.02	0.04	19.67	-
140	0.15	0.25	16.53	2.7
255	0.26	0.27	12.84	42.9
278	2.77	5.07	11.33	76.5
343	2.84	4.07	10.95	84.2
446	0.56	0.74	15.77	83.5
525	0.01	0.02	18.47	78.3
711	0.00	0.01	19.69	69.3

Table S2. Energy spectrum of $^6H_{15/2}$ multiplet for **1b**.

Energy (cm^{-1})	g_x	g_y	g_z	Angle (°)
0	0.02	0.03	19.67	-
161	0.29	0.42	16.51	1.4
286	2.84	5.32	11.63	54.0
326	2.36	4.11	10.39	63.1
374	3.98	4.48	11.76	87.7
420	1.23	1.79	17.59	65.3
499	0.10	0.14	18.04	71.8
598	0.04	0.05	19.29	63.7

Table S3. Energy spectrum of $^6H_{15/2}$ multiplet for **1c**.

Energy (cm^{-1})	g_x	g_y	g_z	Angle (°)
0	0.03	0.04	19.61	--
142	0.27	0.47	16.29	4.5
231	1.33	1.40	15.55	60.7
267	1.30	5.85	9.68	43.3
323	4.10	5.59	9.56	84.0
418	0.69	1.13	15.20	84.8
471	0.14	0.36	18.48	79.1
637	0.00	0.01	19.72	64.0

Table S4. Energy spectrum of $^6H_{15/2}$ multiplet for **2**.

Energy (cm^{-1})	g_x	g_y	g_z	Angle (°)
0	0.00	0.00	19.81	--
219	0.11	0.13	16.92	2.3
420	1.14	2.17	12.31	5.3
488	1.40	4.39	13.59	86.9
554	1.55	2.36	11.91	77.9
580	1.29	3.55	14.63	70.9
612	1.49	2.50	14.93	67.3
792	0.05	0.08	19.49	67.2

Table S5. Energy spectrum of $^6H_{15/2}$ multiplet for **3(Dy1)**.

Energy (cm^{-1})	g_x	g_y	g_z	Angle (°)
0	0.03	0.04	19.50	--
90	0.40	0.54	16.45	12.4
168	3.49	5.61	10.31	49.7
196	0.26	5.65	10.13	88.6
234	1.58	2.47	16.13	86.2
264	1.12	2.20	13.67	70.9
290	1.03	4.71	14.71	85.4
433	0.03	0.03	19.71	55.4

Table S6. Energy spectrum of $^6H_{15/2}$ multiplet for **3(Dy2)**.

Energy (cm^{-1})	g_x	g_y	g_z	Angle (°)
0	0.05	0.05	19.56	--
83	0.48	0.52	16.51	0.9
183	0.62	0.83	12.34	13.4
222	2.91	4.38	13.32	73.6
263	2.54	5.38	11.98	84.2
292	0.62	2.23	17.45	87.3
311	0.37	2.05	16.35	78.8
502	0.00	0.01	19.71	66.6

Table S7. Energy spectrum of $^6H_{15/2}$ multiplet for **4**.

Energy (cm^{-1})	g_x	g_y	g_z	Angle (°)
0	0.09	0.12	19.43	--
68	0.63	0.66	16.45	9.6
161	1.94	3.17	11.08	14.8
198	1.03	6.71	10.97	83.9
254	2.36	4.31	13.09	90.0
276	0.22	0.55	18.73	80.0
342	0.10	0.29	19.07	66.2
457	0.04	0.07	19.65	61.1

Table S8. Energy spectrum of $^6H_{15/2}$ multiplet for **5**.

Energy (cm^{-1})	g_x	g_y	g_z	Angle (°)
0	0.07	0.11	19.36	--
79	0.80	0.98	16.38	15.6
182	1.45	3.47	10.65	6.8
213	0.93	7.33	10.02	65.7
283	1.47	3.90	14.22	88.9
333	0.03	1.58	17.20	77.6
373	0.55	2.33	15.91	72.2
490	0.15	0.21	19.36	73.0